

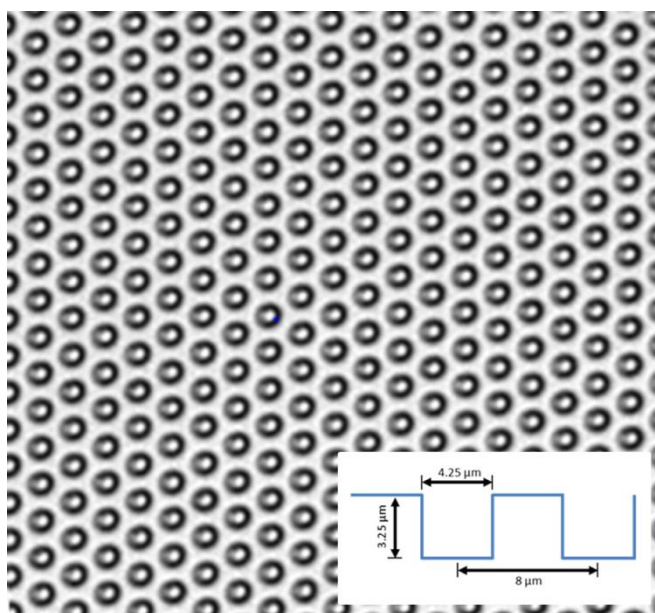
Supporting information

Single-molecule mechanistic study of enzyme hysteresis

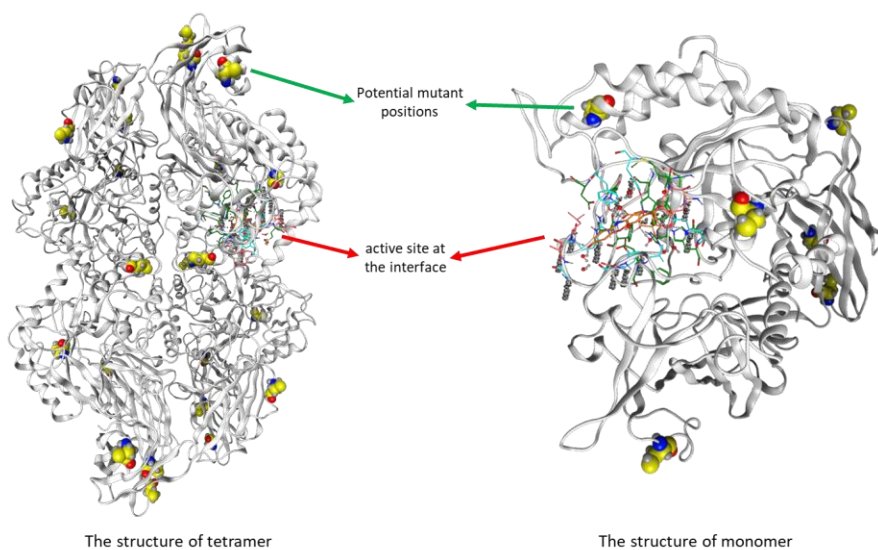
Yu Jiang, Xiang Li, Barrett R. Morrow, Arti Pothukuchy, Jimmy Gollihar, Richard Novak, Charles B. Reilly, Andrew D. Ellington*, David R. Walt*

Table of Contents

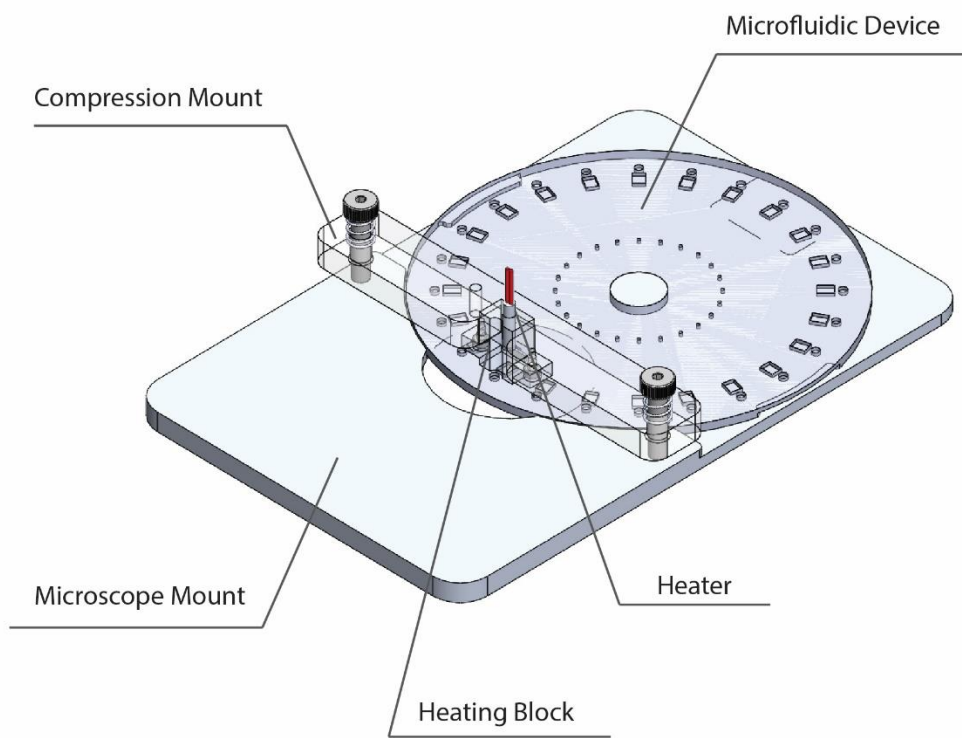
Scheme S1	Microwell array configuration.
Scheme S2	Crystal structure of the WT GUS.
Scheme S3	<i>In situ</i> heating platform.
Table S1	All types of variant GUS.
Figure S1	SDS-PAGE gel image of synthesized GUS protein.
Figure S2	The MALDI-TOF Mass spectrometry result of the GUS protein.
Table S2	Proteomics results of the GUS proteins.
Figure S3	Hysteresis behavior of D1, D2, C262 and C133 variant GUS, compared to WT GUS on plate reader.
Figure S4	Steady-state reaction rate vs. substrate concentration of WT GUS.
Figure S5	Single-molecule initial rate distributions of active WT, C133, and D2 at different time points.
Figure S6	Kinetics of WT and C133 GUS at 25 °C and 37 °C in plate reader.
Figure S7	Calibrating the fluorescence intensity of resorufin standard solution in microliter plate wells(a) and femtoliter chamber(b).
Figure S8	The distribution of initial turnover rate of WT GUS within the first 5 min.
Figure S9	The distribution of initial turnover rate of C133 molecules that are activated at different time points or activated by heat-pulse.
Table S3	The average initial turnover rate of WT and C133 molecules from Figure S8 and Figure S9.
Figure S10	Lack of reversibility of mutant GUS activation.
Figure S11	Hysteresis behavior of D2.
Figure S12	The effect of <i>ex situ</i> heat-pulse imposed on mutant GUS in the presence of substrate.
Figure S13	20 ns molecular dynamics simulation of structures generated via homology modeling, using the WT crystal structure as a template.
Figure S14	The cross activation between two substrates in bulk assays.



Scheme S1. Microwell array configuration. The image was acquired using microscope (10× objective) under white light. The microwell array disk was purchased from Quanterix (MA, USA) and used as received. Each array contains 216,000 microwells. The scheme at bottom right shows the dimensions of each microwell: 4.25 μm diameter, 3.25 μm height, 8 μm center-to-center distance.



Scheme S2. Crystal structure of the WT GUS (PDB ID:3k46). The potential mutations are indicated in yellow and all of the mutations avoided the active site.



Scheme S3. *In situ* heating platform. The heating block was connected to the heater by wires.

Names of mutant GUS	Positions of the mutations
D1	C28K, C133D, C197D, C253V, C527M
D2	C28L, C133D, C197D, C253V, C527M
C262	C28S, C133S, C197S, C527S
C133	C28S, C197S, C262S, C527S

Table S1. All types of variant GUS.

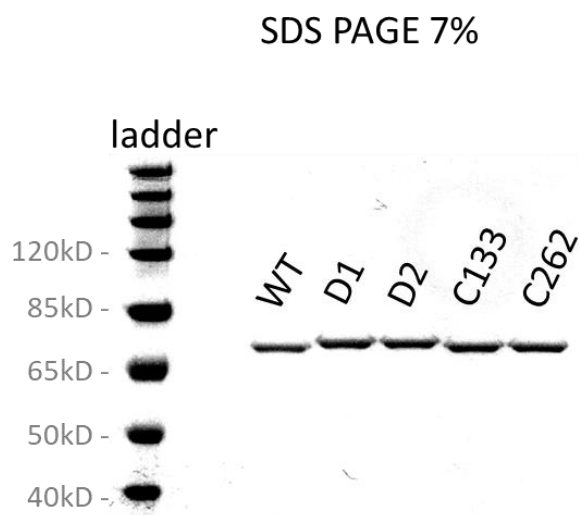


Figure S1. SDS-PAGE gel image of synthesized GUS protein. 2 μ g of each of the GUS variants was loaded into each lane of the gel. The SDS-PAGE electrophoresis result shows that all the proteins centered around 70 kD, which is consistent with the calculated molecular weight of the GUS monomer.

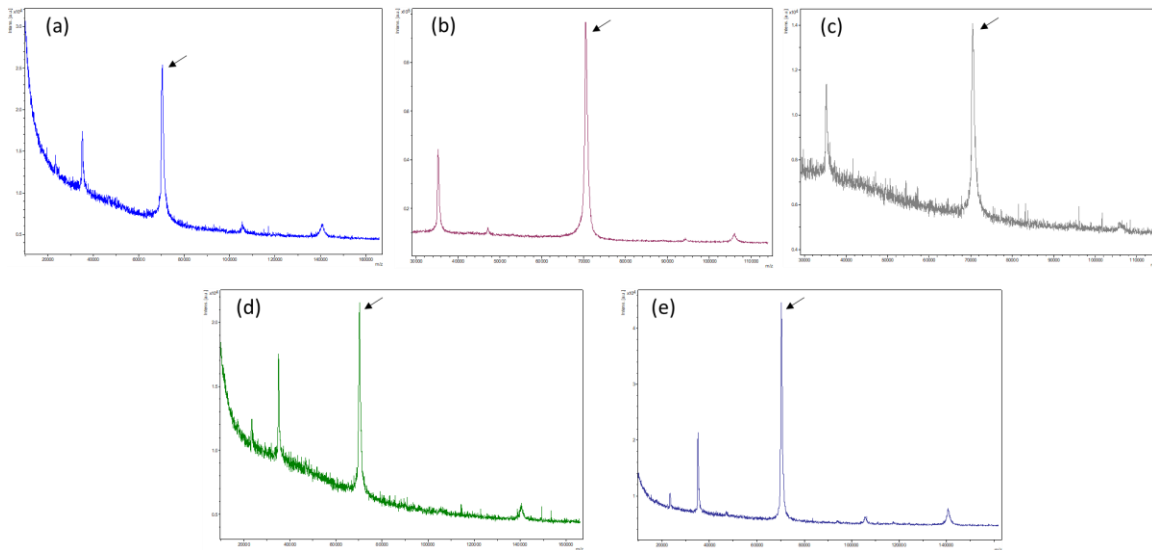


Figure S2. The MALDI-TOF Mass spectrometry results of the GUS protein. (a)to(e) are the mass spectrometry results of WT, D1, D2, C133 and C262, respectively. The peak around 70 kD (indicated by arrows in each sub-figure) was a single peak for all the synthesized GUS proteins, which proves that there is no amino acid loss or damage during expression.

Enzyme	Proteomics coverage	Amino acids confirmed at mutant positions
WT	95.19%	5/5
D1	92.73%	5/5
D2	92.87%	4/5
C133	96.35%	4/4
C262	94.53%	4/4

Table S2. Proteomics results of the GUS proteins.

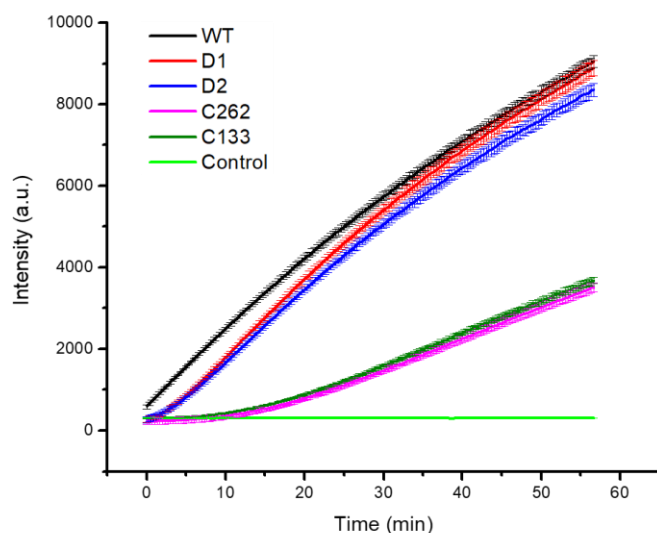


Figure S3. Hysteresis behavior of D1, D2, C262 and C133 GUS variants, compared to WT GUS using a plate reader. The error bars reflect the standard deviations of triplicate measurements with the plate reader. The enzyme concentration was 36 pM and substrate concentration was 100 μ M. The control curve was obtained by monitoring the fluorescence signal of a solution containing 100 μ M substrate only.

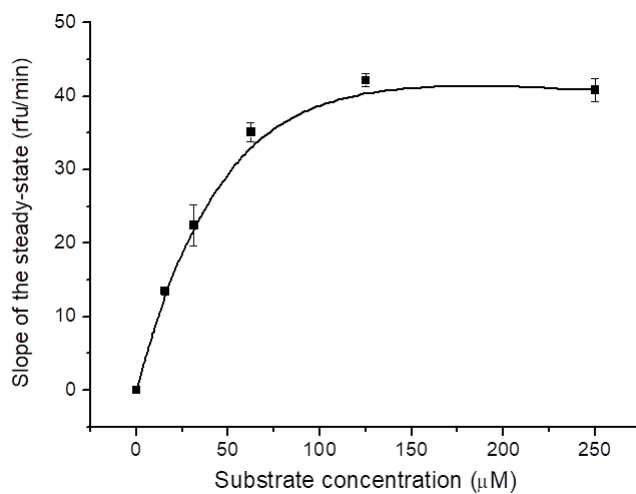


Figure S4. Steady-state reaction rate vs. substrate concentration of WT GUS. The K_m was calculated to be 60.7 μ M. The catalytic rate reaches a maximum when the concentration is higher than 100 μ M. The error bars reflect the standard deviation of triplicate measurements with a plate reader.

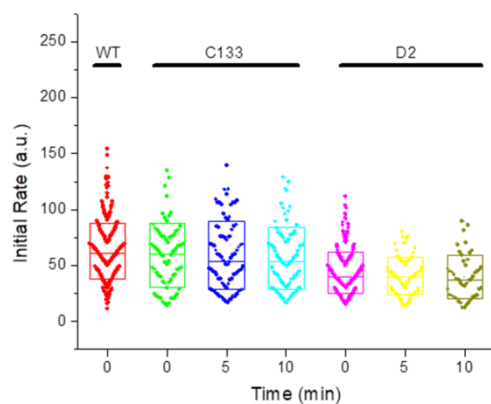


Figure S5. Single-molecule initial rate distributions of active WT, C133, and D2 at different time points. The initial reaction rate was defined as the F_{well} between images that shows the microwell transiting from inactive to active states.

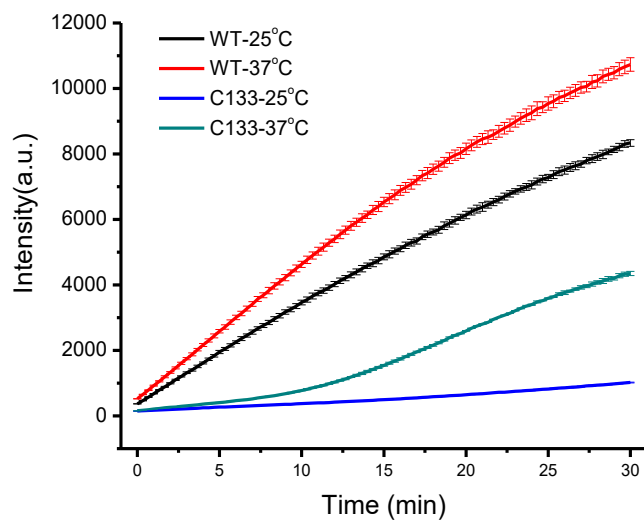


Figure S6. Kinetics of WT and C133 GUS at 25 °C and 37 °C in a plate reader. Each reaction contains 100 pM enzymes and 100 μ M substrate. The error bars reflect the standard deviation of triplicate measurements in the plate reader.

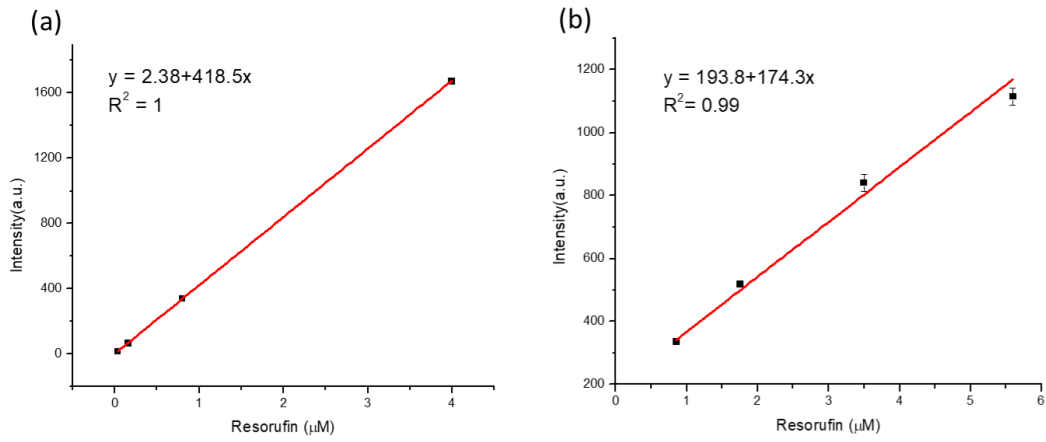


Figure S7. Calibrating the fluorescence intensity of resorufin standard solution in microliter plate wells(a) and femtoliter chambers(b).

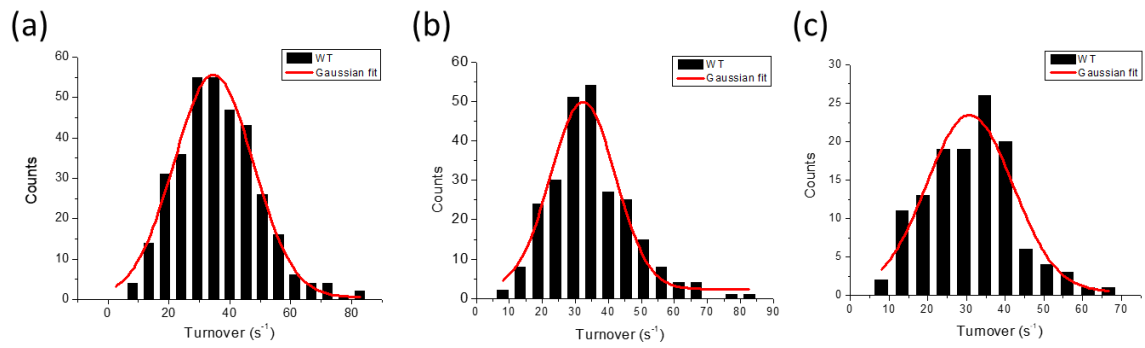


Figure S8. The distribution of initial turnover rates of WT GUS within the first 5 min. (a) to (c) are from the triplicate measurements.

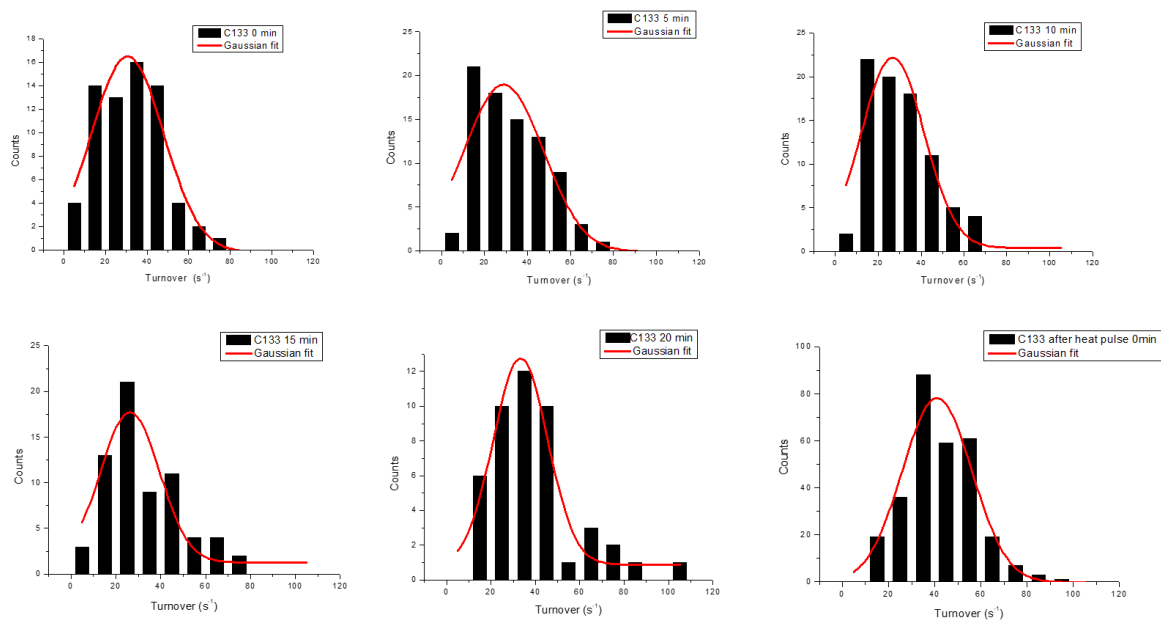


Figure S9. The distribution of initial turnover rates of C133 molecules that are activated at different time points or activated by heat pulse.

Enzyme	Time points of activation	$k_{i,ave}$ (s ⁻¹)
WT	0 min	32
C133	0 min	31
	5 min	29
	10 min	27
	15 min	26
	20 min	33
	Heat pulse 0min	41

Table S3. The average initial turnover rates of WT and C133 molecules from Figure S8 and Figure S9.

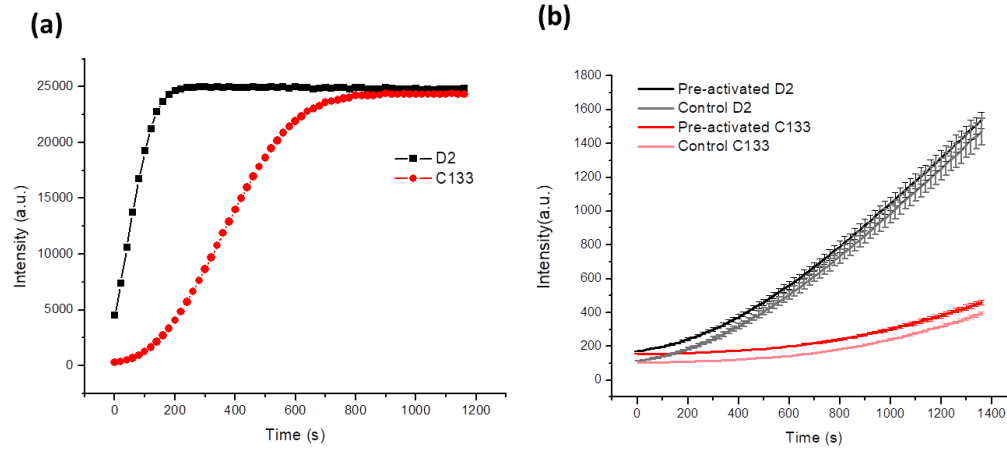


Figure S10. Lack of reversibility of mutant GUS activation. (a) In the pre-activation step, 3.6 nM D2 or C133 were mixed with 100 μ M RDG substrate to pre-activate the enzyme. After reacting for 20 min, the fluorescence intensity reaches a plateau and the substrate should be depleted. (b) In the measurement step, the pre-activated solutions from (a) were diluted 100 fold and allowed to react with 100 μ M newly added substrate. Control samples were obtained with the same procedure, except that the substrate solution was replaced with buffer in the pre-activation step. The error bars reflect the standard deviation of triplicate measurements.

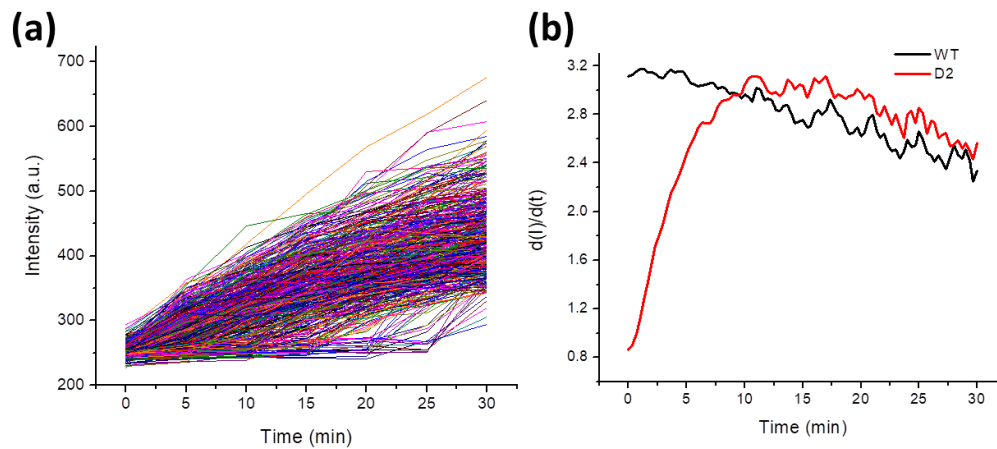


Figure S11. Hysteresis behavior of D2. (a) Single-molecule kinetic traces of D2 measured with microwell array. (b) The derivative of intensity of WT and D2 from Figure S2 vs. time based on the kinetic results from the plate reader.

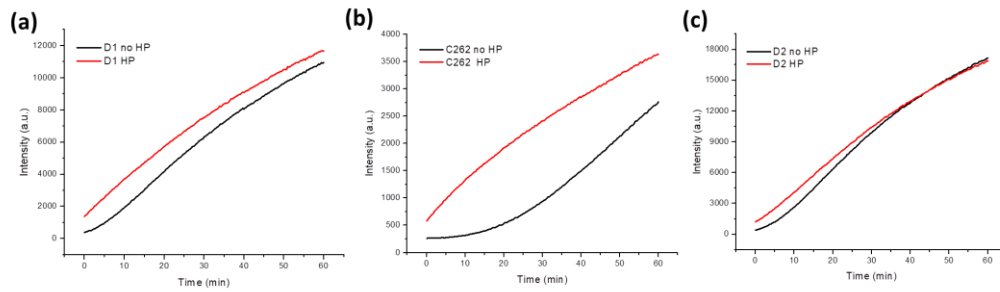


Figure S12. The effect of *ex situ* heat-pulse imposed on mutant GUS in the presence of substrate. The kinetic plots are obtained from 36pM of (a) D1, (b) C262 and (c) D2 and 100 μ M substrate reacting in bulk solution. All the black curves represent the kinetics of reaction without heat-pulse (HP) treatment and all the red curves represent the kinetics of reactions that have gone through HP treatment.

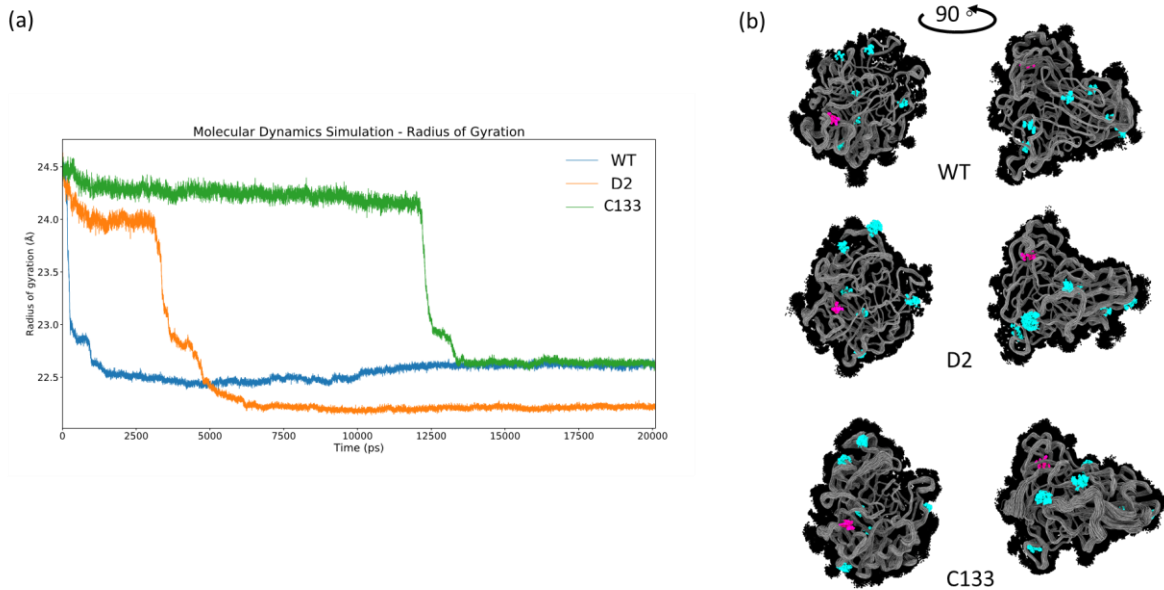


Figure S13. 20 ns molecular dynamics simulation of structures generated via homology modeling, using the WT crystal structure as a template. (a) The radius of gyration of the alpha carbons. (b) Conformations from every 100 ps in the last 5 ns of the MD are superimposed. Mutated residues and the active site residues are colored magenta and cyan respectively.

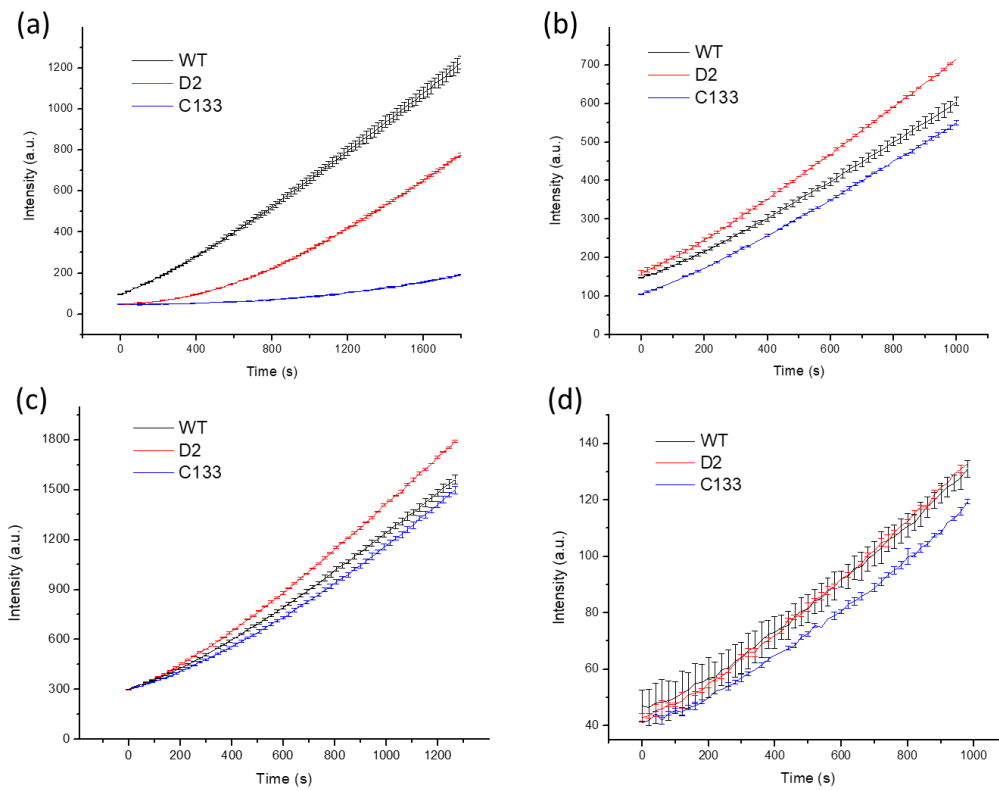


Figure S14. The cross activation between two substrates in bulk assays. (a) The kinetics of 36 pM of three types of GUS reacting with 100 μ M 4-mug. (b) Three types of GUS were pre-heated at 37°C with 100 μ M 4-mug for 1 min before the kinetic reading at 25°C. (c) The kinetics of 4-mug pre-activated GUS reacting with 100 μ M RDG. (d) The kinetics of RDG pre-activated GUS reacting with 100 μ M 4-mug. The error bars reflect the standard deviation of triplicate measurements in the plate reader.